ELSEVIER

Surface Science 499 (2002) 24–40

SURFACE SCIENCE

www.elsevier.com/locate/susc

Theory of the growth mode for a thin metallic film on an insulating substrate

David Fuks [a,*], Simon Dorfman [b,c], Yuri F. Zhukovskii [d,e], Eugene A. Kotomin [d,f], A. Marshall Stoneham [e]

[a] *Materials Engineering Department, Ben Gurion University of the Negev, P.O. Box 653, Beer-Sheva 84105, Israel*
[b] *Department of Physics, Technion—Israel Institute of Technology, Haifa 32000, Israel*
[c] *Department of Physics and Astronomy, Northwestern University, Evanston, IL 60208, USA*
[d] *Institute of Solid State Physics, University of Latvia, 8 Kengaraga Strasse, Riga LV-1063, Latvia*
[e] *Center for Materials Science, Department of Physics and Astronomy, University College London, Gower Strasse, London WC1E 6BT, UK*
[f] *Max Planck Institut für Festkörperforschung, Heisenbergstrasse, 1, Stuttgart 70569, Germany*

Received 13 July 2001; accepted for publication 19 October 2001

Abstract

We have developed a novel theory predicting the growth mode of a thin metallic film on an insulating substrate. This combines ab initio electronic structure calculations for several ordered metal/insulator interfaces (varying both coverage and substrate lattice constant), with a thermodynamic approach based on microscopic calculations. We illustrate this approach for Ag film deposited on MgO(0 0 1) substrate. Ab initio calculations predict high mobility of adsorbed silver atoms on the perfect magnesia surface even at low temperatures. Our theoretical analysis clearly demonstrates that the growth of metallic islands is predominant at the initial stage of silver deposition, which agrees with the experimental data. © 2001 Published by Elsevier Science B.V.

Keywords: Ab initio quantum chemical methods and calculations; Equilibrium thermodynamics and statistical mechanics; Growth; Coatings; Magnesium oxides; Silver

1. Introduction

Systems in which a metal is deposited on a ceramic continue to grow in importance and in the variety of their uses. In applications, whether as catalysts, in recording media, in metal-matrix composites, or in their various microelectronic uses, the morphology of the metal is often crucial. Yet there remain widely varying views as to the nature of the metal–ceramic interfacial binding and of the microscopic mechanism of metal film growth [1–3]. The pattern (i.e., the microstructure and morphology) of metal films deposited on oxides proves to depend strongly on growth conditions, especially for thin layers. The growth mode usually falls into one of three categories: layer-by-layer; formation of a three-dimensional (3D)

* Corresponding author. Tel.: +972-7-461460; fax: +972-7-6461460/472946.
E-mail address: fuks@bgumail.bgu.ac.il (D. Fuks).

0039-6028/01/$ - see front matter © 2001 Published by Elsevier Science B.V.
PII: S0039-6028(01)01692-2

metal island; growth to a layer and then to islands [4]. Which mode occurs can be determined by energetics, by kinetics, or by a mixture of these two.

How does one predict the morphology? Even for a single layer of metal atoms, before the traditional growth patterns, such as island growth, are fully established. Traditionally, there have been three types of approach. One is a kinetic approach, based on specific assumptions about the motion and energetics of small clusters of metal atoms [4]. This is a powerful method at small adatom concentrations, where there are relatively few crucial groupings of adatoms and processes. A second approach, mainly used in other fields, is to draw parallels with spinodal decomposition, and to seek the fastest-growing instability that defines the way to reach the most probable stable state with different clusters on the surface. The free energy, F in a binary solid solution is a function of the component concentration, c. The curve $F(c)$ may include concave and convex parts. An alloy of a composition corresponding to a point on the convex part of the curve $F = F(c)$ (i.e., $d^2F/dc^2 < 0$) cannot be stable against decomposition into a two-phase mixture. Since the range where the curve $F(c)$ is convex may be chosen infinitesimally small, a homogeneous solid solution is unstable at $d^2F/dc^2 < 0$ with respect to an infinitesimal concentration heterogeneity within the infinitesimal range of concentrations, $c_1 < c < c_2$. This instability is usually called spinodal instability, and the corresponding decomposition reaction is called spinodal decomposition. The line that describes the boundary of the spinodal instability region in the T–c diagram where $d^2F(c,T)/dc^2 = 0$ is called the spinodal curve. More details on spinodal decomposition may be found in Ref. [5]. The second approach is more useful for behavior at constant composition, whereas many experiments relevant to our work vary the adatom density on a timescale which can be similar to the timescale of the instability. We adopt a third approach, recognizing that phase diagrams are more than a very effective way to summarize equilibrium data. Phase diagrams provide a guide to reaching desirable non-equilibrium structures. We shall predict the main features of such a phase diagram. In addition, we shall assess whether or not diffusion is likely to be rate limiting.

Equilibrium growth modes are characterized mainly by the thermodynamics of the system, although some features may depend on kinetic factors, such as the rate of deposition and the competition between different surface processes. The growth of an Ag film on an MgO(0 0 1) substrate usually gives rise to 3D metallic islands [6,7] which begin to appear at Ag coverages above some critical value (varying from one experiment to another from 0.1 to 0.5 ML [8,9]). However, some low-energy-electron-diffraction studies (LEED) found metastable layer-by-layer growth for Ag deposited on vacuum-cleaved MgO(0 0 1) surfaces [10,11]. A delicate energy balance between 3D island and monolayer growth modes was also established in recent calculations [12]. Structural surface defects play a role in determining the growth mechanism, since defects can markedly increase the interface strength [13,14]. Moreover, the initial nucleation of two-dimensional (2D) Ag clusters at low submonolayer coverage probably occurs at some defects on the MgO surface [9]. Whatever is the mechanism and the competing processes, it is important to know the structures that are most stable thermodynamically. Knowing this, even for a metal film on a defectless oxide substrate, identifies a limit to which the system will finally strive, even when kinetics drives another structure. The thermodynamic limit for the ideal system further provides a reference system for detailed studies of realistic, defective surfaces.

Despite much theoretical work on the adhesion of noble and transition metals on regular MgO substrates [15–28], using widely varying models and computational methods, there is still a lack of full understanding of interface formation and of interface properties on an atomic scale. Partly this is because there are sensitive balances between contributions to the energy of metal on an oxide substrate. Both of the traditional ab initio formalisms of Hartree–Fock (HF) and density functional theory (DFT) have been used to calculate the electronic structure explicitly. Finite-cluster models of the metal/MgO interfaces were studied both by HF [15,16] and DFT [17,18] methods. Periodic slab models of the same systems have

mainly used variants of DFT [19–24], based on local spin density (LSD) and generalized gradient approximations (GGA) approaches. Partly to study effects of the exact exchange in slab calculations of Ag/MgO(0 0 1) and Ag/MgO(011) interfaces, a series of HF calculations with a posteriori electron correlation corrections (HF-CC) was published recently [25]. Two simpler atomistic methods, the image interaction model (IIM) and the shell model (SM), have been successfully applied to Ag/MgO interfaces. IIM simulations combined image interaction calculations between the substrate ions and a free-electron metal with a Fermi cutoff, with HF calculations of short-range interactions between the metal atoms and ion cores [26]. When using the SM, containing several hundreds of relaxed atoms, different kinds of interatomic potentials have been exploited [27]. In spite of many differences between these ab initio and semi-empirical simulations, several common conclusions can be drawn. The interaction between the atoms of transition and noble metals and a defect-free MgO substrate is characterized as comparatively weak *physisorption*, with the adhesion energy smaller than 0.5 eV (theoretically determined adhesion energies are likely to exceed the appropriate experimental values because of misfit dislocations, which reduce the measured adhesion energy [1]).

Concerning applicability of the kinetic Monte-Carlo (MC) simulations to the study of the metallic film growth on surfaces, readers are referred to the book and recent review [29]. Briefly, MC calculations are based on transferable intersite interactions. These latter depend on which sites are occupied by a particular species, unlike interatomic potentials, which depend on the precise coordinates of the atoms involved; the distinction is significant in other contexts, such as H in metal systems [30]. It is very difficult to derive empirical potentials for MC simulations in our specific case of determining the growth mode of thin metallic films, partly because the nature of the interaction changes as relative amount of metal increases. Non-empirical potentials could be useful here, but it is not a trivial task to determine or to model even partial Ag–Ag interactions in the vicinity of a substrate. This interaction is not the same as in the bulk Ag, and cannot easily be obtained empirically from experimental data for surfaces. Simple considerations show that the situation is even more dramatic. The ab initio calculations predict quite noticeable charge redistribution even in the vicinity of regular interface [14,25]. The empty sites in the above-substrate metal layer, which is partly filled by Ag atoms, have an effective charge. This leads to an interaction between the empty sites (E) themselves, and also to the interaction of E sites with Ag atoms. Thus, partial potentials for E–E and Ag–E interactions are also essential for MC simulations. An analogous problem arises for the Ag–Mg and Ag–O potentials needed for MC interface simulations. In principle, one could extract interatomic potentials from experimental data for molecules, but these will not be the same interactions as those we need. They may have little in common with those from the bulk alloys, as noted. Last, but not least, MC only simulates the situation that might occur if the monolayer was already formed. As a rule, MC accounts for finite number of interactions only in a few coordination shells of atoms.

In this paper, we use the results of ab initio HF-CC calculations on the electronic structure of a regular Ag/MgO(0 0 1) interface as a basis for the development of a thermodynamic scenario to understand a metal film initiation and growth mode on an insulating support at different temperatures. Although our general methodology was recently briefly formulated in Ref. [31], this paper complements the latter study with the essential physical background. Thus, we supplement our pilot study [31] with the analysis of the role of different factors in the thermodynamics of interfacial system. This analysis demonstrates several important aspects in modeling the coating of MgO substrate by Ag atoms: (1) we present the results of the calculations of adhesion energy for Ag/MgO interface using different electron correlation corrections (LSD- and GGA-type) and substrate models (one- and two-side adsorption on three- and five-layer slabs, respectively); (2) we study the charge re-distribution for different positions of Ag atoms atop MgO(0 0 1) surface and show that the bonding mechanism for silver adlayer–magnesia substrate is physisorption; (3) we calculate by means

of direct ab initio modeling the diffusion of Ag along the MgO surface, show its high mobility and fast approach to the thermodynamic equilibrium when the metallic monolayer is formed; (4) we present the formalism that allows to make a choice between the superstructures that may be, in principle, formed in 2D metallic layer above the MgO substrate; this formalism is based on the symmetry considerations and being combined with our ab initio results allows to predict the morphology of 2D Ag–E solid solution; (5) we prove that the thermodynamic scenario of silver monolayer formation on MgO(0 0 1) surface is a spinodal decomposition in 2D Ag–E solid solution; (6) lastly, we analyze the sensibility of thermodynamic predictions to the details of ab initio modeling.

2. Ab initio simulation for the ordered Ag/MgO(0 0 1) interface

2.1. Theoretical background

In our theoretical simulation of the perfect MgO substrate, we have considered finite-thickness slabs with 2D periodicity. Since the Ag coverage of the MgO(0 0 1) surface was varied from 1/4 metal layer (1:4 coverage) to a monolayer (1:1 coverage), we have made series of calculations for the 2×2 extended surface unit cells of magnesia slabs. These allow us to model four kinds of Ag structures on the Ag/MgO(0 0 1) interface, as shown in Fig. 1. In our previous studies, we have found and explained why silver atoms adhere preferentially to the O-site on the MgO(0 0 1) surface [25]. Indeed, such a metal/oxide interface configuration agrees well with experiment [6–9]. Thus, we shall consider Ag over O-sites on MgO as appropriate for all four structures, which are: silver monolayer (Fig. 1a), two regular configurations of 1:2 Ag coverage (Fig. 1b and c), and 1:4 coverage (Fig. 1d). Our choice of the structures presented by Fig. 1b–d is dictated by symmetry consideration (see Section 3). In constructing effective site interaction potentials for thermodynamic simulations of Ag film growth on an MgO(0 0 1) substrate, for all of these structures we have carried out total energy optimization. For the metal/oxide system, this is a 2D

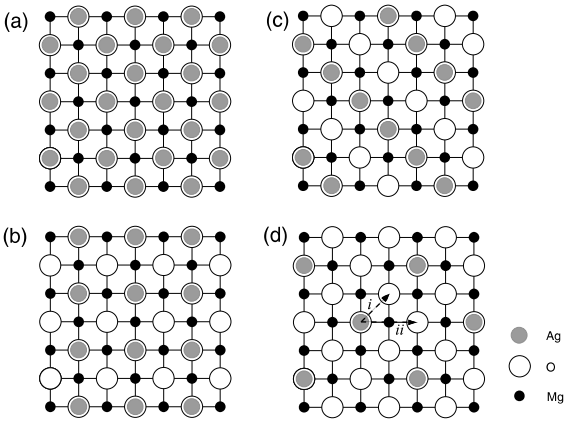

Fig. 1. Top view of the MgO(1 0 0) surface with different superstructures of Ag atoms placed atop it. Images correspond to Ag coverages of (a) 1:1 (a regular monolayer), (b) 1:2 (a square distribution), (c) 1:2 (a striped distribution), and (d) 1:4 (quasi-isolated metal atoms), respectively. Directions marked as *i* and and *ii* denote two trajectories of possible surface diffusion of Ag atoms.

optimization of the total energy $E_{\mathrm{tot}}(a_{\mathrm{MgO}}, d_{\mathrm{Ag-O}})$ as a function of the substrate lattice constant a_{MgO} and the interface distance $d_{\mathrm{Ag-O}}$. For the MgO substrate, we optimize the total energy $E_{\mathrm{tot}}(a_{\mathrm{MgO}})$ as a function of lattice constant.

We used a periodic slab model containing either three or five MgO(0 0 1) layers with one- and two-side silver adhesion, respectively. As in earlier studies on the three-layer substrate [25], we neglect surface relaxation of magnesia slab, which is known to be small [32]. For both models containing one and two Ag adlayers, the corresponding adhesion energy per atom (E_{adh}) is defined according to the universal binding energy relation [21,25].

In our ab initio calculations we use the HF-CC formalism as implemented in the CRYSTAL98 code [34], with a wide choice of various a posteriori electron correlation corrections to the total energy. Using this method, we could describe adequately a wide spectrum of properties for both regular and defective Ag/MgO(0 0 1) interface [14, 25]. Although a standard HF approach usually overestimate bond length and underestimate the binding energy per chemical bond, the correlation corrections certainly do improve quality of HF

calculations on the total energy [35]. The applicability of different electron correlation functionals, based on both GGA and LSD approximations, to the concrete system is established by a careful analysis of the corresponding computational data (Tables 1–3). In the present paper, we have analyzed not only Perdew–Wang (PWGGA) correlation corrections [36], as earlier, but also other kinds of correlation functionals, both GGA-type (Lee–Yang–Parr [37]) and LSD-type (Perdew–Zunger [38] and Vosko–Wilk–Nusair [39]). This is important, since we compare results of our HF-CC calculations with other theoretical studies, obtained using DFT methods based on both LSD and GGA exchange and correlation functionals. The basis sets (BS) for Mg, O, and Ag, and some other computational details are the same as in our previous papers in which we calculated the atomic and electronic structure of defective and perfect monolayers, and three-layer Ag/MgO(0 0 1) interfaces [14,25]. We use the same BS, but we have estimated more carefully the basis set superposition errors (BSSE) for different configurations of Ag/MgO(0 0 1) interfaces according to CRYSTAL98 computational scheme [34].

2.2. Results and discussion

Now we present results of the latest ab initio calculations, going somewhat beyond our recent simulations of the regular Ag/MgO(0 0 1) interface [25]. These new data (Table 1) are essential for our further thermodynamic treatment.

The value of the lattice constant for the pure MgO(0 0 1) substrate optimized for a 2×2 supercell has been found to be smaller than in our previous calculations for the bulk unit cell. We find this value in the range 4.09–4.15 Å for various correlation functionals and adhesion models, to be compared with the previous result 4.21 Å [25] and with the experimental bulk value 4.205 Å [32]. One component of the difference comes from the surface stress which like the surface tension of a liquid, tends to reduce the interatomic spacing. This

Table 1
Main results of the HF-CC simulation on the Ag/MgO(0 0 1) interface

Optimized parameters of calculations	Different a posteriori electron correlation corrections and substrate models							
	Perdew–Wang GGA		Lee–Yang–Parr GGA		Perdew–Zunger LSD		Vosko–Wilk–Nusair LSD	
	Three-layer[a]	Five-layer[a]	Three-layer[a]	Five-layer[a]	Three-layer[a]	Five-layer[a]	Three-layer[a]	Five-layer[a]
Pure MgO(0 0 1) surface								
a_{MgO} (Å)	4.09	4.11	4.10	4.12	4.13	4.14	4.12	4.14
1:4 Ag coverage of MgO(0 0 1) surface (Fig. 1d)								
a_{MgO} (Å)	4.09	4.10	4.09	4.11	4.13	4.13	4.13	4.14
d_{AgO} (Å)	2.58	2.59	2.59	2.60	2.63	2.64	2.64	2.65
E_{adh} (eV)	0.23	0.22	0.22	0.21	0.20	0.19	0.19	0.18
1:2 Ag coverage of MgO(0 0 1) surface (a square distribution, Fig. 1b)								
a_{MgO} (Å)	4.08	4.10	4.09	4.10	4.12	4.13	4.12	4.13
$d_{Ag–O}$ (Å)	2.58	2.58	2.59	2.59	2.62	2.63	2.63	2.64
E_{adh} (eV)	0.23	0.22	0.22	0.21	0.20	0.20	0.20	0.19
1:2 Ag coverage of MgO(0 0 1) surface (a striped distribution, Fig. 1c)								
a_{MgO} (Å)	4.08	4.09	4.09	4.10	4.12	4.12	4.12	4.13
$d_{Ag–O}$ (Å)	2.69	2.69	2.68	2.69	2.74	2.76	2.73	2.75
E_{adh} (eV)	0.12	0.11	0.12	0.11	0.10	0.10	0.10	0.09
1:1 Ag coverage of MgO(0 0 1) surface (Fig. 1a)								
a_{MgO} (Å)	4.07	4.08	4.08	4.08	4.12	4.13	4.12	4.13
$d_{Ag–O}$ (Å)	2.55	2.56	2.56	2.56	2.60	2.61	2.61	2.61
E_{adh} (eV)	0.26	0.25	0.25	0.25	0.22	0.21	0.21	0.20

[a] Three- and five-layer magnesia slabs are used in the models of one-side and two-side silver adhesion, respectively.

Table 2
The internal formation energies (eV) for three superstructures shown in Fig. 1b–d[a]

U (eV)	Different a posteriori electron correlation corrections and substrate models							
	Perdew–Wang GGA		Lee–Yang–Parr GGA		Perdew–Zunger LSD		Vosko–Wilk–Nusair LSD	
	Three-layer	Five-layer	Three-layer	Five-layer	Three-layer	Five-layer	Three-layer	Five-layer
U_1	0.552	0.518	0.566	0.474	0.433	0.408	0.426	0.409
U_2	1.031	1.058	1.029	0.973	0.865	0.906	0.865	0.904
U_3	0.828	0.821	0.843	0.782	0.716	0.718	0.716	0.718

[a] The correlation functionals are the same as in Table 1.

Table 3
The sensitivity of the Fourier transform of the mixing potential $\widetilde{V}(0)$ (eV) to the choice of the correlation corrections (the same as in Table 1)[a]

Perdew–Wang GGA	Lee–Yang–Parr GGA	Perdew–Zunger LSD	Vosko–Wilk–Nusair LSD
−2.791	−2.828	−2.830	−2.944

[a] Data for the three-layer slab at different a posteriori electron correlation corrections.

effect can be seen from the systematic differences of about 0.02 Å between three-layer and five-layer systems. The interface distances between silver atoms and substrate have been optimized using the $E_{\mathrm{tot}}(a_{\mathrm{MgO}}, d_{\mathrm{Ag\text{–}O}})$ function for all four structures shown in Fig. 1. The influence of this optimization on the energy parameters for the phases given in Fig. 1b–d will be discussed in Section 4A. As the Ag coverage increases from 1:4 to 1:1, the equilibrium $d_{\mathrm{Ag\text{–}O}}$ distance decreases negligibly, by $<3\%$ (Table 1) and is accompanied by the adhesion energy increase by 0.03–0.04 eV. For all used correlation functionals, the Ag adhesion energy lies between 0.18 and 0.26 eV per adatom, showing that we have physisorption. The adhesion energy is even smaller (a less stable interface) for the case of the striped 1:2 Ag coverage shown in Fig. 1c, where $d_{\mathrm{Ag\text{–}O}}$ is larger than for other configurations (Table 1). Using the LSD-type correlation functionals, the equilibrium values of both a_{MgO} and $d_{\mathrm{Ag\text{–}O}}$ are found to be slightly larger, but the corresponding values of E_{adh} smaller than those for the GGA-type functionals. These trends are typical for HF-CC and DFT methods implemented in CRYSTAL98 code [34].

The BSSE corrections [40] were found to be quite small (0.01–0.02 eV per adatom); they are included in results presented in Table 1. The lateral interactions between adjacent Ag atoms are rather small for 1:4 and even 1:2 square coverages shown in Fig. 1b and d, respectively. This is why their stable configurations have practically the same values of E_{adh}. However, these lateral interactions are more significant for the striped configuration (Fig. 1c), which is clearly energetically unfavorable, and so has larger interfacial distances (Table 1). In the case of the two-side adhesion model, the corresponding values of E_{adh} are slightly smaller, but the equilibrium interface distances are nearly the same as for the one-side case. This confirms that interaction between Ag atoms positioned on the two opposite sides of the slab is negligibly small and that three-layer substrate slab is thick enough for further modeling using one-side adhesion model.

When simulating possible trajectories for surface diffusion of silver atoms, we have used the lowest (1:4) metal coverage where Ag atoms are well separated. Two energetically preferable diffusion trajectories are shown in Fig. 1d: (i) along the [1 1 0] direction, beginning with silver atom placed above substrate oxygen ion, then it hops over a gap position to the next one over substrate O^{2-} ion; (ii) along the [1 0 0] direction, starting with the same position above the substrate O^{2-} ion, then hopping over the substrate Mg^{2+} ion, Ag atom comes again atop the next substrate oxygen ion. We will use below the corresponding energy barriers along these trajectories in the estimate how Ag mobility affects the growth mode of thin metallic film. The mean square displacement

of Ag atom could be defined in a standard way [33]:

$$\langle r^2 \rangle_{\mathrm{Ag}} = 4\tau D_0 \exp\left(-\frac{\epsilon}{kT}\right), \quad (1)$$

where $D_0 \exp(-\epsilon/kT)$ is the diffusion coefficient depending on the migration activation barrier ϵ and the temperature T, D_0 and k are the diffusion pre-factor and the Boltzmann constant, respectively, whereas τ is the time necessary for mutual approach and aggregation of mobile Ag atoms. Using Eq. (1), we can compare the rate of adatom diffusion with the rates of other processes.

The energy barrier ϵ for the Ag atom diffusion along the [1 1 0] direction (Fig. 1d) turns out to be very small, about 0.05 eV (found with PWGGA correlation corrections in our HF-CC calculations). For the alternative diffusion pathway along the [1 0 0] direction, the diffusion barrier is higher ($\approx$0.12 eV with the same CC), reducing the probability of this diffusion path. As a result, we predict Ag atoms to be highly mobile, even at low temperatures. If we use these activation energies ϵ in Eq. (1) at $T \sim 300$ K together with a typical D_0 value of 10^{-3} cm^2 s^{-1} and a surface coverage of about 0.1, we obtain a characteristic time $\tau \sim 10^{-6}$ s for diffusion-controlled aggregation of Ag atoms on the MgO(0 0 1) surface. This value suggests a fast process of Ag aggregation. It is interesting to note that a small diffusion barrier for Ag atoms on quite different Pt(1 1 1) surface was also recently found in ab initio calculations [41].

In order to analyze the electron charge redistribution in the vicinity of the interface, we have sectioned slabs of both Ag monolayer and 1:4 layer on the MgO(0 0 1) substrate along the (1 0 0) plane, which *ii*-projection is shown on Fig. 1d. The difference electron density maps shown in Fig. 2 are drawn with respect to a superposition of interacting and isolated silver and magnesia slabs.

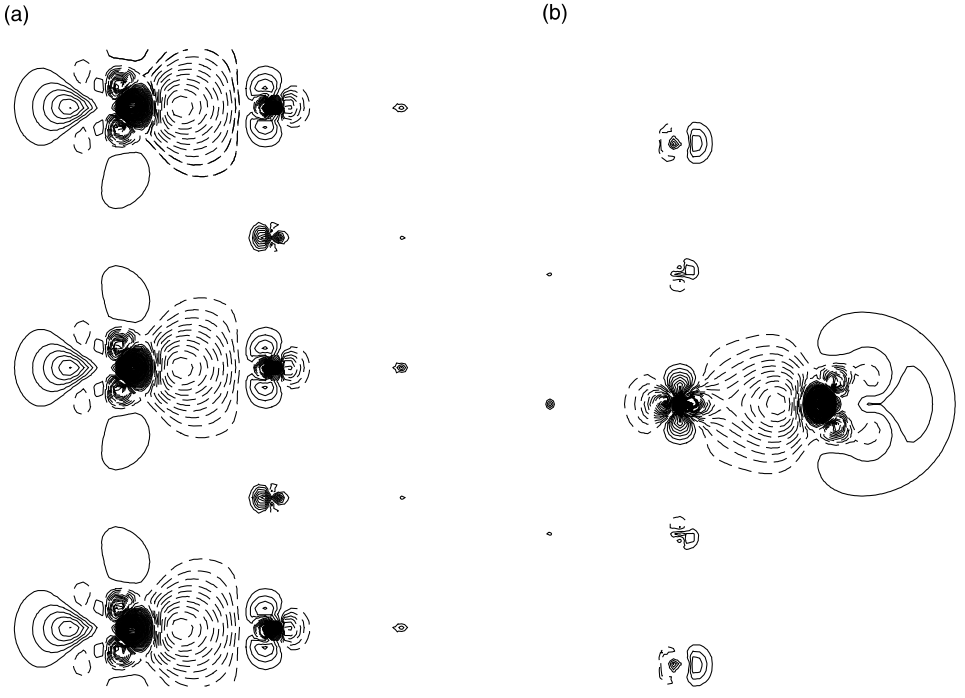

Fig. 2. Two difference charge distribution maps (the total electron density for the Ag/MgO(0 0 1) interface minus superposition of the same densities for isolated Ag and MgO slabs) along the (1 0 0) cross-section perpendicular to interface: (a) for monolayer silver coverage (Fig. 1a) and (b) for 1/4 Ag adlayer (Fig. 1d). Density isolines are drawn from -1.0 to 1.0 e au^{-3} with an increment of 0.005 e au^{-3}.

There is significant electron charge redistribution in the vicinity of silver/magnesia interface (Fig. 2), indicating a marked polarization of the interacting Ag atom and of the nearest substrate O^{2-} ion. However, the charge transfer from substrate to metal atoms is very small (varied between 0.06*e* for 1:4 and 0.04*e* for 1:1 coverages), whereas the electron charge on surface Mg^{2+} ions remains almost unchanged. Population analysis clearly shows absence of any chemical bonding across the interface. For a silver monolayer, it is an enhanced electron density between adjacent Ag atoms, which increases the adhesion energy [25] (Fig. 2a).

3. Thermodynamic theory

3.1. Formalism

Now we develop a statistical thermodynamic approach as the next step in theoretical modeling of the Ag monolayer formation on the MgO(0 0 1) surface. This formalism we shall combine with our ab initio atomistic calculations discussed in Section 2. As follows from our microscopic study, a series of first-principles calculations [16–21,25], and experimental data [6–9], (1) Ag atoms prefer the sites above oxygen ions in the adlayer coating on MgO(0 0 1), rather than above Mg^{2+} ions; and (2) the equilibrium distance between the Ag adlayer and magnesia surface is essentially independent of the concentration of adsorbed Ag atoms. These circumstances allow us to study the formation of Ag film as a 2D system consisting of Ag atoms and "empty sites". This system is formed on a planar lattice placed above the MgO(0 0 1) substrate; the sites of this lattice are situated above oxygen ions, and the lattice is immersed in the field of the electronic charge distribution created by the magnesia surface. The adatom monolayer structure with some sites of 2D lattice occupied by Ag atoms could be described as 2D "solid solution", Ag–E, which is formed by Ag atoms and empty site quasi-particles, E. The thermodynamics of such solid solution may be formulated with the help of the effective mixing site interactions potential

$$\widetilde{V}(\vec{r},\vec{r}') = V_{\mathrm{Ag\text{–}Ag}}(\vec{r},\vec{r}') + V_{\mathrm{E\text{–}E}}(\vec{r},\vec{r}') - 2V_{\mathrm{Ag\text{–}E}}(\vec{r},\vec{r}'), \tag{2}$$

where $V_{\mathrm{Ag\text{–}Ag}}(\vec{r},\vec{r}')$, $V_{\mathrm{E\text{–}E}}(\vec{r},\vec{r}')$, and $V_{\mathrm{Ag\text{–}E}}(\vec{r},\vec{r}')$ are the effective site interactions potentials between silver atoms, between quasi-particles, and between silver atoms and quasi-particles, respectively; $\vec{r}$ and $\vec{r}'$ are the positions of the sites in 2D lattice. The mixing site interactions potential (2) describes the interactions in such a 2D system in the field of semi-bulk MgO terminated by a free (0 0 1) surface.

The atomic fractions of Ag atoms or of E quasi-particles in this 2D solution can be determined in the usual way. The total number of particles in this system is conserved, being equal to the number of 2D lattice sites. This simplifies the application of a traditional thermodynamic theory of substitutional solid solutions, when, let us say, Ag atoms substitute for E quasi-particles. The analysis of thermodynamic stability of this 2D solid solution becomes a study of the ordering and/or decomposition tendencies in such a binary system on the 2D Ising lattice, and the stability may be considered in terms of the phase diagram of 2D-alloy. This method of investigation has been used for different systems, including single crystal surfaces, magnetic systems, systems with long-range repulsive interactions or purely attractive interactions (see, for example Ref. [42,43], and references therein). We shall use the concentration wave (CW) approach, developed in Ref. [44]. This theory has several advantages over other statistical theories of alloys. One advantage is that CW theory uses Fourier transforms of interatomic interaction potentials that are site interactions potentials in our case. Thus, it accounts formally interactions in all coordination shells, and does not make the common approximation of the first or the first and the second neighbor interactions, i.e. the nearest neighbors approximation.

In this theory the distribution of atoms A in a binary alloy is described by a single occupation probability function $n(\vec{r})$. This function gives the probability of finding the atom A (Ag) at the site $\vec{r}$ of the crystal lattice. The configurational part of the free energy of formation of 2D solid solution per atom is given by

$$F = \frac{1}{2N}\sum_{\vec{r},\vec{r}',\vec{r}\neq\vec{r}'} \widetilde{V}(\vec{r},\vec{r}')n(\vec{r})n(\vec{r}') + kT\sum_{\vec{r}}\{n(\vec{r})\ln[n(\vec{r})] + [1-n(\vec{r})]\ln[1-n(\vec{r})]\}. \quad (3)$$

The summation in Eq. (3) is performed over the sites of the 2D Ising lattice. The function $n(\vec{r})$, which determines a distribution of solute atoms in an ordering phase, may be expanded in Fourier series. It is presented as a superposition of CWs,

$$n(\vec{r}) = c_A + \tfrac{1}{2}\sum_{j_s,s}[Q(\vec{k}_{j_s})e^{i\vec{k}_{j_s}\vec{r}} + Q^*(\vec{k}_{j_s})e^{-i\vec{k}_{j_s}\vec{r}}], \quad (4)$$

where c_A is concentration of particles A (Ag in our case), $e^{i\vec{k}_{j_s}\vec{r}}$ is a CW, k_{j_s} is a non-zero wave vector defined in the first Brillouin zone of the disordered binary alloy, the index $\{j_s\}$ enumerates the wave vectors in the Brillouin zone, that belong to the star s, and $Q(\vec{k}_{j_s})$ is a CW amplitude. As shown in Ref. [43], all $Q(\vec{k}_{j_s})$ are linear functions of long-range-order (LRO) parameters of superlattices that may be formed on the basis of the Ising lattice of the disordered solid solution:

$$Q(\vec{k}_{j_s}) = \eta_s\gamma_s(j_s). \quad (5)$$

Here η_s are LRO parameters, and $\gamma_s(j_s)$ are coefficients that determine the symmetry of the occupation probabilities $n(\vec{r})$ (the symmetry of the superstructure) with respect to a rotation and reflection symmetry operations. The LRO parameters are defined in such a way that, in a completely ordered state, where $n(\vec{r})$ are either unity or zero on all lattice sites $\{\vec{r}\}$, all parameters η_s should be equal to unity. This requirement completely defines the constants $\gamma_s(j_s)$. The definition of the LRO parameters coincides with the conventional definition in terms of the occupation probabilities of sites in the different sublattices. Substitution of Eqs. (4) and (5) into the first term of Eq. (3) gives the internal energy of formation per atom for the ordering superstructure in a form

$$U = \tfrac{1}{2}\widetilde{V}(0)c_A^2 + \tfrac{1}{2}\sum_{j_s,s}\eta_s^2\gamma_s^2(j_s)\widetilde{V}(\vec{k}_{j_s}), \quad (6)$$

where $\widetilde{V}(\vec{k}_{j_s})$ is the Fourier transform of the mixing site interactions potential and $\widetilde{V}(0)$ is the same for the vector $\vec{k}_{j_s}$ equal to zero. Eqs. (3) and (6) define the Helmholtz free energy and the internal energy of ordering phases with respect to the reference state. We are emphasizing that the advantage of the expression (6) in the use of Fourier transforms that makes possible to include long-range interactions associated with a substrate strain.

3.2. Application to 2D solid solution Ag–E on (0 0 1) MgO surface

In simulations of a coverage of MgO(0 0 1) surface by a layer of Ag atoms, we have chosen the 2D-structures given in Fig. 1. The case in Fig. 1a corresponds to $c_A = 1$: full surface coverage; there are no CWs in this structure. According to Eq. (4) occupation probabilities for the 2D lattice structures shown in Fig. 1b–d could be calculated after carrying out vectors $\vec{k}_{j_s}$. The superstructure vectors $\vec{k}_{j_s}$ define positions of additional X-ray reflections that appear within the disorder–order transformation of the binary system. This transformation leads from a disordered state on the Ising lattice to an ordered or partly ordered state. The vectors determine new unit translations in the reciprocal lattice arising from the reduction of the translation symmetry caused by the ordering. These vectors describe the structures, which have the minimum of $V(\vec{k})$ from the symmetry considerations. To choose these vectors, the Lifshitz criterion [45] is used. According to this criterion the point group of the vector $\vec{k}_{j_s}$ contains the intersecting elements of symmetry. The ordering of the disordered Ag–E solid solution on the 2D lattice in structures displayed in Fig. 1b and c is described by only one vector $\vec{k}_{j_s}$. The superstructure vector $\vec{k}_1 = 2\pi/a(1,0)$ defines the structure displayed in Fig. 1b. The structure shown in Fig. 1c is defined by the vector $\vec{k}_{2_1} = (2\pi/a)((1/2),(1/2))$, while the structure shown in Fig. 1d is described by the combination of three CWs with vectors $\vec{k}_{j_s}$:

$$\vec{k}_1 = \frac{2\pi}{a}(1,0), \quad \vec{k}_{2_1} = \frac{2\pi}{a}\left(\frac{1}{2},\frac{1}{2}\right), \text{ and}$$

$$\vec{k}_{2_2} = \frac{2\pi}{a}\left(-\frac{1}{2},\frac{1}{2}\right).$$

The occupation probabilities for structures shown in Fig. 1 are

$$n_1(\vec{r}) = c_A^{(1)} + \tfrac{1}{2}\eta\, e^{i2\pi x}, \tag{7}$$

$$n_2(\vec{r}) = c_A^{(2)} + \tfrac{1}{2}\eta\, e^{i\pi(x+y)}, \tag{8}$$

$$n_3(\vec{r}) = c_A^{(3)} + \tfrac{1}{4}\eta_1\, e^{i2\pi x} + \tfrac{1}{4}\eta_2\left[e^{i\pi(y+x)} + e^{i\pi(y-x)}\right] \tag{9}$$

where n_1, n_2, and n_3 correspond to Fig. 1b–d, respectively. In Eqs. (7)–(9) x and y are the coordinates of the lattice sites of the Ising lattice and should be substituted in the lattice parameter units. Stoichiometric compositions of these ordering 2D phases are $c_A^{(1)} = c_A^{(2)} = 1/2$, and $c_A^{(3)} = 1/4$. It is easy to check by direct substitution of coordinates of the Ising lattice sites that for displayed structures in absolutely ordered states and stoichiometric compositions the occupation probabilities are equal to unity in the sites where Ag atoms are placed and are equal to zero in the empty sites. The internal energies of formation for these phases are respectively

Fig. 1b:

$$U_1 = \tfrac{1}{2}\widetilde{V}(0)c^2 + \tfrac{1}{8}\widetilde{V}(\vec{k}_1)\eta^2, \tag{10}$$

Fig. 1c:

$$U_2 = \tfrac{1}{2}\widetilde{V}(0)c^2 + \tfrac{1}{8}\widetilde{V}(\vec{k}_2)\eta^2, \tag{11}$$

Fig. 1d:

$$U_3 = \tfrac{1}{2}\widetilde{V}(0)c^2 + \tfrac{1}{32}\widetilde{V}(\vec{k}_1)\eta_1^2 + \tfrac{1}{16}\widetilde{V}(\vec{k}_2)\eta_2^2. \tag{12}$$

It may be shown that the value of the Fourier transform of the mixing site interactions potential, $V(\vec{k}_j)$, is the same for different vectors $\vec{k}_j$ belonging to the same star of vectors (in Eqs. (11) and (12) the notation $V(\vec{k}_2) = V(\vec{k}_{2_1}) = V(\vec{k}_{2_2})$ is used). The last superstructure is described by two LRO parameters. As it was mentioned in the Section 2, the total energies of these superstructures were calculated by means of the ab initio HF-CC method.

4. Application to the Ag/MgO(001) interface

4.1. Analysis of the phase competition

We choose the reference state energy in a conventional way (see, for example, Ref. [46]) as the energy of a heterogeneous mixture of components of the Ag–E solid solution. In our case it is calculated as the sum of weighted (according to atomic fraction) total energies per lattice site for the "empty" lattice and the lattice filled by Ag atoms above the same MgO slab. Keeping in mind that in absolutely ordered state all LRO parameters in Eqs. (10)–(12) are equal to unity, we obtained from the HF-CC calculations using PWGGA correlation functional and three-layer slab model of magnesia substrate (Table 1) the following values: $U_1 \approx 0.552$ eV, $U_2 \approx 1.031$ eV, and $U_3 \approx 0.828$ eV. To clarify the effect of the correlation functionals on energy differences for the ordered phases that define the phase competition, we performed also additional calculations with different electron correlation corrections mentioned in Section 2. The results are shown in Table 2. The dispersion in the calculated energies does not exceed 25% for any of these quite different correlation corrections, and this consistency is enough for our qualitative conclusions about mechanisms of thin film growth mode. As follows from Table 2 the thickness of the underlying magnesia slab also does not affect significantly. As may be seen from Table 2 the energies U_1, U_2 and U_3 calculated for optimized lattice parameter of the 3L or 5L slab and for the optimized distance between Ag layer and substrate change only a little for each of investigated correlation corrections models. For example, for PWGGA model U_1 changes in 6%, while the changes in U_2 and U_3 are even less significant. The main result remains unchanged: all three energies U_1, U_2, and U_3 are always positive (for all investigated models of correlation corrections and for optimized lattice parameter of the 3L and 5L slabs). This means that the states represented by the phases considered (Fig. 1b–d) have a higher energy than the reference state. Thus the *decomposition* of Ag–E solid solution should occur. All considered phases are unstable with respect to decomposition, they are unfavorable as compared with the heterogeneous mixture of components in Ag–E. The diffusion of Ag atoms along the surface cannot stabilize these phases. Even the most favorable absolutely ordered phases are unstable. Any jump of Ag atoms from their "regular" sites to "irregular" sites in Ag–E ordered phase will result in partial disorder. This process will make these

phases less favorable, and the solid solution will decompose. On the other hand, if the diffusion that held in disordered solid solution will lead to formation of some ordered regions in Ag–E with the Ag–E phases considered in Fig. 1b–d, they will be thermodynamically unstable and should decompose. Thus the coupling of two Ag atoms with the loss of symmetry cannot lead to the stabilization of the phases given by Eqs. (7)–(9). It worth to mention that the energy of the considered phases is calculated in terms of Fourier transforms of interatomic potentials $V_{\mathrm{Ag-Ag}}$, $V_{\mathrm{Ag-E}}$, and $V_{\mathrm{E-E}}$. The energy of phases, and thus the potentials, are defined in the field of the underlying MgO substrate slab with (0 0 1)-terminated surface. The same potentials determine the energy barriers in Ag adatom diffusion. In this sense we have self-consistency in the definition of the energy characteristics of the phases and the energy barriers for Ag adatom diffusion that were presented in Section 2.2.

At the same time, the obtained data allow us to calculate the energy parameter needed to describe the decomposition in Ag–E solid solution. Solving Eqs. (10)–(12) for the parameters $\widetilde{V}(0)$, $\widetilde{V}(\vec{k}_1)$, and $\widetilde{V}(\vec{k}_2)$ we get $\widetilde{V}(0) \approx -2.791$ eV for PWGGA correlation functional and three-layer magnesia slab. For the five-layer slab with the same correlation corrections we get $\widetilde{V}(0) \approx -2.604$ eV that as compared with aforementioned result obviously demonstrates that three-layer slab is enough for thermodynamic predictions—the variation of the energy parameter is about 7%. This result proves also that the polarization effects are small in the case of Ag/MgO system. In these calculations we have assumed that energy parameters $\widetilde{V}(0)$, $\widetilde{V}(\vec{k}_1)$, and $\widetilde{V}(\vec{k}_2)$ are concentration-independent. This assumption is based mainly on the results of the diffuse X-ray scattering data for the alloys (see Ref. [47]). Table 3 illustrates the sensitivity of the key energy parameter, Fourier transform of the mixing potential $\widetilde{V}(0)$, to the choice of correlation functionals used in the calculations with three-layer MgO slab. It is well seen that $\widetilde{V}(0)$ does not vary by more than 10% when different correlation corrections are used.

The condition $n(\vec{r}) = c_{\mathrm{A}} = \text{constant}$ corresponds to the case of disordered 2D solid solution when all LRO parameters in Eqs. (6)–(8) are equal to zero. Substitution of $n(\vec{r}) = c_{\mathrm{A}}$ into Eq. (2) gives the free energy of this solution

$$F(c) = \frac{1}{2}\widetilde{V}(0)c^2 + kT[c\ln c + (1-c)\ln(1-c)], \tag{13}$$

where we have omitted the index A. From the simple thermodynamic consideration, it follows that an equilibrium phase diagram remains unaffected if the free energy given by Eq. (13) is replaced by

$$F(c) = -\frac{1}{2}\widetilde{V}(0)c(1-c) + kT[c\ln c + (1-c)\ln(1-c)]. \tag{14}$$

This expression includes the chemical potential term, and is more convenient because of its symmetry with respect to $c = 1/2$. The 2D phase diagram of the Ag–E disordered solid solution calculated with Eq. (14) is given in Fig. 3. It has the miscibility gap, and the decomposition reaction takes place because the obtained value $\widetilde{V}(0) < 0$.

4.2. Phase diagram for 2D solid solution

The calculated phase diagram represents the case of the limited solid solubility in a binary 2D

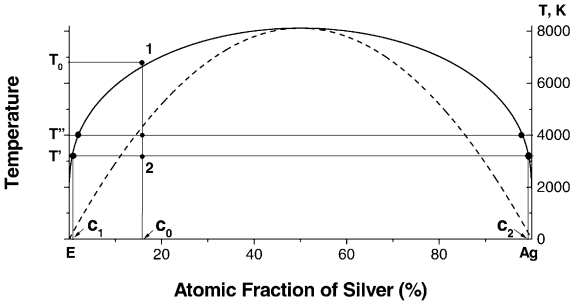

Fig. 3. The calculated phase diagram of the Ag–E 2D solid solution. The bold line is a solvus and the dashed line is a spinodal. The existence of the solid solution is assumed in the given temperature range. The system is single-phase above the solvus line (point 1), and decomposes into two-phase state below the spinodal line (point 2) at temperature T'. A line at T'' illustrates conditions leading to increase of Ag contents in a phase with low silver concentration and to decrease of Ag contents in silver-enriched phase. At T'' a fraction of Ag-enriched phase decreases in comparison with T'.

Ag atom-quasi-particle solution. The solvus is shown in Fig. 3 by the solid line, and the dashed line describes the spinodal. The solubility curve is determined by the necessary minimum condition $dF(c)/dc = 0$. The spinodal curve is given by the equation $d^2F(c)/dc^2 = 0$. According to the suggested model, the two-phase region is symmetric with respect to concentration $c = 1/2$. This follows from the assumption that energy parameter is concentration independent. To analyze the decomposition in the solid solution, let us start from the point 1 on Fig. 3. This point represents the high-temperature state of a metal monolayer with an equilibrium concentration of Ag atoms c_0 at the temperature T_0. This is a single-phase state, corresponding to the disordered solid solution in the monolayer, when Ag atoms randomly occupy the sites of the 2D lattice atop oxygen ions of the MgO(0 0 1) surface. Cooling of the system to temperature T' takes us to the state shown by point 2, below the spinodal.

After annealing at this new temperature T' the equilibrium two-phase state of the solid solution is obtained. The thermodynamic mechanism of the formation of this state is a decomposition of the single-phase state into the two-phase state. This two-phase state is a mixture of two random solid solutions in the Ag–E system. One phase is an extremely dilute solid solution of metal atoms, randomly distributed on the lattice sites with the equilibrium concentration c_1 (phase 1). The second phase is also a random solid solution of the same type as the first one, but with extremely high concentration of Ag atoms, c_2 (phase 2). Thus, the two-phase state represents the mixture of the phases: one is highly enriched with Ag, whereas the second one is depleted of Ag atoms. The relative fraction of the phase 2 in a two-phase mixture is defined by the lever rule, and is equal to $(c_0 - c_1)/(c_2 - c_1)$, whereas the fraction of the phase 1, with its smaller concentration of Ag atoms, is much higher, and is equal to $(c_2 - c_0)/(c_2 - c_1)$. If the solubility regions are narrow, we shall have a very small fraction of the phase 2. Nevertheless, this phase has to exist. The two-phase state that corresponds to the temperature T' and atomic fraction c_0 is characterized therefore as Ag-rich regions which are immersed in a 2D monolayer lattice with few Ag atoms and many empty sites randomly distributed over the rest of the surface. These small Ag-rich regions are also random solid solutions (Ag–E), but the concentration of Ag in them is very large and the number of empty sites correspondingly small.

The lever rule makes it possible to find the "volume" fraction of the phases co-existing at each alloy composition if the equilibrium phase diagram is known. Making use of this rule, it is easy to understand the changes in the structure of the two-phase state. When the temperature increases from T' to T'' the point c_1 in the Fig. 3 moves to the right and c_2 moves to the left. This will decrease the fraction of the Ag clusters, i.e. the fraction of the phase enriched by Ag, and increase simultaneously the fraction of the extremely dilute Ag–E solid solution. At the same time the atomic fraction of Ag atoms in clusters decreases, that means the increase of the empty sites in these clusters.

Let us consider now the case when after cooling from the temperature T_{01} (points 1 or 3 in Fig. 4) to the temperature T_1' the system comes to the region of the phase diagram between the solvus and the spinodal (points 2 or 4 in Fig. 4). It is easy to see from Eq. (14) that the condition $d^2F(c)/dc^2 > 0$ is satisfied in this region of the phase diagram. For all points c' inside this interval the curve $F(c')$ is concave, and this condition means that the

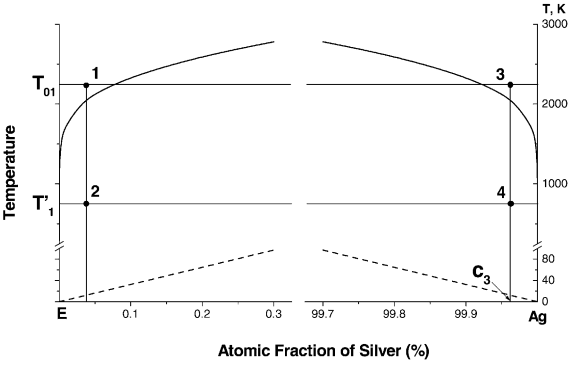

Fig. 4. A part of the phase diagram of Fig. 3 enlarged in the vicinity of the concentration corners. The system is metastable between the solvus and spinodal lines with respect to nucleation and growth of metal clusters. See description of marks in the text.

homogeneous solid solution is stable with respect to infinitesimal heterogeneity. Indeed, if $d^2F(c)/dc^2 > 0$ it is always possible to choose an infinitesimal region of concentrations $c'_1 < c' < c'_2$ in the vicinity of the point c', where $d^2F(c)/dc^2 > 0$, i.e. where the curve $F(c)$ is concave. This curve lies below the straight line connecting the points $\{c'_1, F(c'_1)\}$ and $\{c'_2, F(c'_2)\}$. Therefore the homogeneous single-phase alloy is more stable than a mixture of two phases having infinitesimally different compositions.

If a homogeneous alloy characterized by the condition $d^2F(c)/dc^2 > 0$ at the point c is unstable with respect to the formation of the two-phase mixture with c_α and c_β phase compositions that are substantially different from the alloy composition, the alloy is stable nevertheless with respect to infinitesimally small composition heterogeneity. This is a metastable alloy, and the described situation corresponds to the points 2 and 4 in Fig. 4. The decomposition reaction in this case should involve the formation of finite composition heterogeneity and follow the nucleation-and-growth mechanism. A small increase of the atomic fraction of Ag beyond the value c_3 (see Fig. 4) to the right from the solvus curve will leave the Ag–E solid solution in single-phase state. The system will also remain in single-phase state if the temperature T is changed to bring the "alloy" to the state above the solvus.

Thus, following our discussion, we can formulate a simple thermodynamic rule for the processing of the Ag coating on an MgO(0 0 1) surface. The Ag-rich clusters will be obtained at low Ag coverage if the process is such that, at the end, the system exists in the region of the phase diagram between the solvus and spinodal with subsequent decomposition into a two-phase state. A more-or-less "monolayer" state will be obtained if, at the end, the system finds itself in the region below the spinodal on the phase diagram. In the first case, further coating by Ag will lead to the growth of 3D silver clusters on the substrate surface, since those clusters existing already in a monolayer serve as nuclei for such a growth. At the same time, the thermodynamic stability conditions prohibit the 2D growth of clusters already existing in a monolayer. In the second case, if the system exists below the spinodal in Fig. 4 (with a high atomic

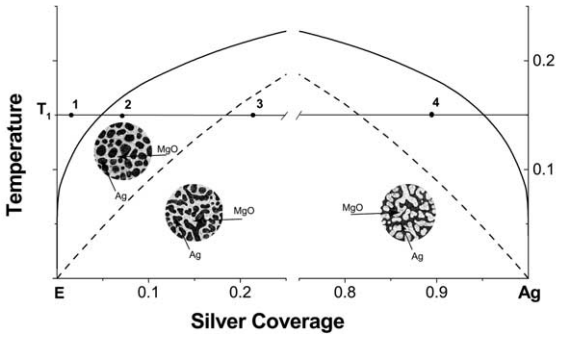

Fig. 5. Phase diagram for the Ag film growth on the MgO(0 0 1) substrate at low temperature. The round frames show the typical morphology for spinodal (under the dashed curve) and cluster (between the solid and dashed curves) decompositions. Black areas are Ag, grey ones are MgO. Temperatures are in units of $k/|\tilde{V}(0)|$. See description of the marks in the text.

fraction of Ag atoms), a low-quality quasi-monolayered structure may be formed. The coverage will have almost uniform structure, but be a two-phase state, nevertheless. This is illustrated by the picture in the right round frame in Fig. 5. At very high temperatures, coating by Ag atoms will leave the system in a one-phase state, namely a disordered Ag–E solid solution with a high concentration of Ag atoms. During the process, if the fraction of Ag atoms is very high, one may expect the formation of a single-phase state that is presented by a good monolayer. This monolayer is a random Ag–E solid solution but with very high fraction of Ag atoms (and thus, a small fraction of empty sites). It is difficult to reach the thermodynamic equilibrium in this single-phase state at low temperature because the solubility region at rather low temperature T'_1 in Fig. 4 is extremely narrow. At the same time, if the necessary thermodynamic conditions are satisfied, the metal monolayer may grow up. Then the formation of the next monolayer above the first, stable layer may begin. This will develop as a layer-by-layer growth process. We would like to emphasize that the same growth mechanism may also be realized for high Ag coverage if the system is below the spinodal. In this case, however, the "monolayer" will not be uniform enough. It will not have the structure of well-separated Ag clusters, nor will it be a one-phase state.

Fig. 5 could be used for a better understanding of our predictions for the silver film growth on magnesia substrate. When covering the MgO(0 0 1) surface by Ag atoms with a fixed deposition rate, at $T = T_1$ in Fig. 5, we start at very low coverages with the random Ag distribution over the surface (point 1). At metal concentrations above fractions of percent we move already into the region 2 of a metastable solid solution, where very small metal clusters are formed. Further increases of a metal coverage bring us to the point 3, representing predominant range of Ag concentrations, where in the equilibrium the system is in a two-phase state.

If the system passes from this region into a single-state mode, with randomly distributed Ag atoms of increasing concentration, it has a small chance to remain in this state also close to $c = 1$. This would result in a metal layer-by-layer growth mode. However, the most probable scenario is that the system will decompose into two phases, with fast Ag cluster nucleation in the region of point 4. If so, the further increase of silver concentration would lead only to the growth of Ag clusters (probably 3D) serving as nuclei for further aggregation. The decomposition reaction in this case involves the formation of finite composition heterogeneity and follows the nucleation-and-growth mechanism. Particles of the Ag-rich phase that are formed in this region of the phase diagram are well separated. They have low connectivity and may be considered as isolated Ag clusters. This situation is typical for decomposition of binary dilute solid solution with limited solubility [48,49]. It is very likely that this results in growth of 3D metal islands.

4.3. Comparison with experimental data

The kinetics of the single-phase decomposition is controlled mainly by long-range diffusion of single silver atoms into metal clusters. As we estimated above, the characteristic time for silver atom diffusion and aggregation on a lattice covered by one percent of Ag at 100 K turns out to be as short as 10^{-6} s, so that makes efficient Ag aggregation to be a very fast process. Note that the nucleation and growth kinetics have been discussed intensively in the literature, see, e.g., Ref. [4]. In the previous paragraphs, we have described the spinodal decomposition of the Ag–E dilute solid solution in the low-temperature region. If we look at the E-rich side of phase diagram, we can describe the data from real experiments [10] in terms of decomposition. The analogous decomposition pattern was observed in the Ag-rich side of the diagram [6]. Electron micrographs presented in both Fig. 6a in Ref. [10] and Fig. 1 in Ref. [6] indeed visualize a spinodal decomposition predicted by our theory. It means that in these experiments substrates were kept at temperatures below the spinodal for Ag–E 2D solid solution. These microstructures are typical for traditional spinodal decomposition morphology (see, e.g., Figs. 2 and 3, and Fig. 6 in Ref. [49] as well as Fig. 4-38a in [48]). Lastly, Fig. 6b in Ref. [10] shows the metal cluster formation region. According to our approach, in this case the system is in the region of the phase diagram located between the solvus and the spinodal. Our approach, combining thermodynamics with ab initio calculations, is supported also by the conclusions of Ref. [50]. The experimental data reported there confirm that thin 2D Ag films grown at room temperature evolve rapidly toward an island structure when raising the temperature just above room temperature. In terms of our phase diagram in Fig. 5, this means that the system transfers from the region below the spinodal to the region between the spinodal and the solvus.

We do understand, of course, that the model depicted for the formation of the metal coating is strongly over-simplified, and that the real equilibrium pattern in the silver film growth on the surface of magnesia might be more complicated. First of all, the mean-field approximation used in our theory, does not account for some fine peculiarities of the phase formation, including the correlation effects (the readers are referred to the special literature devoted to this question [51]). The approximation of pairwise interactions is implicit in our study, even though many-body interactions may play an important role changing the relative energetics of the phases that compete in the phase diagram. Several additional factors may also affect the conditions of the phase formation in the above-studied 2D solid solution. Among them is

3% misfit in the lattice parameters of the pure Ag and the bulk MgO. This means it is necessary to take account for the elastic part of the energy in the minimization of the free energy of 2D-alloy formed at the Ag layer atop the MgO(0 0 1) surface. The structure of the alloy in this case may become more complicated.

It may include some 2D analog of the Guinier–Preston zones that may be formed as in the case of small misfit in 3D metallic alloys [48]. Lattice strains may lead to the formation of strain-modulated structures complicating the morphology of the 2D structures formed in the monolayer. The geometry of the substrate surface underlying the monolayer coating may change the effective field in which the 2D-film is embedded. In this case the phase diagram may change, including, for example, formation of ordered phases that will be favorable with respect to the disordered system or to the decomposition process. The same may happen when the surface of the substrate is alloyed by additional elements, or includes vacancies or extended defects. Each of the above-mentioned factors needs to be the subject of a special investigation. Nevertheless, the approach in terms of the phase diagrams may be still extremely fruitful in understanding the main trends in the equilibrium pattern formation in the metallic monolayers growing on the insulating surfaces.

5. Conclusions

In this paper, we have developed a novel thermodynamic formalism based on ab initio calculations for ordered metal/oxide interfaces. This needs calculations of the metal superstructures with low surface coverages. A novel approach being applied to the Ag/MgO system has enabled us to predict the conditions when the metal atom distribution should be random or when metal atoms aggregate into clusters, and to estimate metal density in such clusters. We proved that for Ag/MgO, in principle, a monolayer metal film could grow via the spinodal decomposition. Our ab initio calculations of the migration barrier for silver atoms moving atop MgO(0 0 1) surface allowed to demonstrate their high mobility which makes metal island formation via nucleation-and-growth mechanism almost unavoidable. Although the growth kinetics is very dependent on the deposition rate of Ag atoms on the surface our study may be considered as complementary to the kinetic approach to the problem [4] in the limit of low deposition rate when the thermodynamic approach should work. We definitely showed that different types of growth modes of thin metallic films on oxide substrates may be treated in the framework of the single theory of decomposition in 2D solid solution. In our specific case of silver adlayer on magnesia substrate this manifests as the spinodal decomposition of the solid solution of Ag atoms and empty sites. Our paper gives a new understanding of different growth modes with the sole mechanism. In contradiction to other approaches, our theory accounts for the bonding not only between Ag atoms but also between Ag atoms and different atoms of the substrate. Moreover, it accounts for the type (crystallography) of the surface where the thin metallic film grows on. This conclusion follows directly from our statement of the problem—the 2D solid solution of Ag atoms is treated explicitly in the field produced by specific surface of the underlying ceramic.

To clarify the effect of the correlation corrections on the relative energies for some ordered phases, which define the phase competition we performed HF-CC calculations with different electron correlation functionals (LSD- and GGA-type) and compared the obtained results. We have shown that variation of the formation energies for considered phases does not exceed 25%, which does not affect the qualitative conclusions. We discussed also the sensitivity of the key energy parameter—Fourier transform of the mixing potential $\widetilde{V}(0)$ to the choice of correlation functionals. The effect of correlation corrections on the value $\widetilde{V}(0)$ is less than 10%. The sign of $\widetilde{V}(0)$ is also remains the same confirming our conclusion about the physisorption mechanism of the formation of silver monolayer.

We have used both one-side adsorption model of the Ag/MgO(0 0 1) interface with different silver coverages of three-layer substrate slab and the two-side silver adsorption over both sides of five-layer MgO(0 0 1) slab. We have analyzed different

structural and electronic properties of both models and did not find essential differences between them. Influence of artificial dipole layer on interface properties is rather negligible.

A novel theory could be applied to many metal/insulator systems, which would permit the prediction of the conditions for a random metal atom distribution, or for metal atom aggregation into clusters, as well as to estimate the metal density in such clusters. Our approach has several advantages as compared with the usual kinetic MC simulations for similar problems:

1. The mixing Ag–E quasi-particle potential is defined in the external field of the substrate. Thus, we account effectively the charge re-distribution effects when the Ag layer grows above some specific plane of magnesia substrate.
2. Use of the mixing site interactions potential, $V(\vec{r},\vec{r}')$, allows one to avoid the problem of explicit definition of the pair site interactions potentials, $V_{\mathrm{Ag–Ag}}$, $V_{\mathrm{E–E}}$ and $V_{\mathrm{Ag–E}}$, because $V(\vec{r},\vec{r}')$ is already the necessary combination of those potentials and is the only quantity needed for thermodynamic theory developed in our paper.
3. The same is true for the Ag–Mg and Ag–O potentials that are necessary for MC simulations of the Ag film growth on MgO substrate. It could be possible to extract such interatomic potentials from the corresponding experimental data for the molecules, but these interactions differ from the same potentials for Ag adatoms. Our mixing energy for the 2D system, on the other hand, is based on an optimization procedure which takes account of the interactions determined in the field of the underlying substrate.
4. As a rule, the MC method accounts the atomic interaction in a very limited number of coordination shells. In our approach we use directly the Fourier transforms of the mixing potentials. It means that the interaction includes contributions from all coordination shells.

Summing up, in this paper we have suggested a new physical approach that allows to explain the effect of external conditions on a growth mode of thin metal films on insulating substrates. This approach is based on the ab initio calculations combined with thermodynamic study of the stability of 2D solid solution "metal atom–empty site". For a particular Ag/MgO(0 0 1) interface, this is the spinodal decomposition. This explains a non-trivial situation observed experimentally. Depending on the temperature and concentration of metal atoms, the metal film could grow as a monolayer or as metal clusters. As we show, this is defined by the condition of metal coverage growth above or below the spinodal line.

Acknowledgements

DF and SD are thankful to G. Borstel and D.E. Ellis for kind hospitality and fruitful discussions. YZ highly appreciates creative atmosphere at the Centre for Materials Science at UCL, London, during his stay there. Authors thank J.H. Harding, E. Heifets, P.W.M. Jacobs and J. Maier for stimulating discussions as well as B. Herschend for preparation of Fig. 2. This study was partly supported by a British–Latvian Royal Society collaborative grant and by European Centre of Excellence for Advanced Materials Research and Technology (contract no ICA1-CT-2000-7007). SD acknowledges the support of the KAMEA program.

References

[1] M.W. Finnis, J. Phys. Cond. Mat. 8 (1996) 5811.
[2] C. Noguera, Physics and Chemistry at Oxide Surfaces, Cambridge University Press, Cambridge, 1996.
[3] C.T. Campbell, Surf. Sci. Rep. 27 (1997) 1.
[4] J.A. Venables, G.D.T. Spiller, M. Hanböcken, Rep. Prog. Phys. 47 (1984) 399;
J.A. Venables, Phys. Rev. B 36 (1987) 4153;
J.H. Harding, A.M. Stoneham, J.A. Venables, Phys. Rev. B 57 (1998) 6715.
[5] M. Hillert, Phase Equilibria, Phase Diagrams and Phase Transformations: Their Thermodynamic Basis, Cambridge University Press, Cambridge, 1998.
[6] A. Trampert, F. Ernst, C.P. Flynn, H.F. Fishmeister, M. Rühle, Acta Metall. Mater. 40 (1992) S227.
[7] M.-H. Schaffner, F. Patthey, W.-D. Schneider, Surf. Sci. 417 (1998) 159.
[8] O. Robach, G. Renaud, A. Barbier, Phys. Rev. B 60 (1999) 5858.

[9] P. Stracke, S. Krischok, V. Kempter, Surf. Sci. 473 (2001) 86;
J.H. Larsen, J.T. Ranney, D.E. Starr, J.E. Musgrove, C.T. Campbell, Phys. Rev. B, in press.
[10] T. Harada, M. Asano, Y. Mizutani, J. Cryst. Growth 116 (1992) 243.
[11] F. Didier, J. Jupille, Surf. Sci. 307–309 (1994) 587.
[12] A.M. Stoneham, J.H. Harding, Acta Mater. 46 (1998) 1155.
[13] A.V. Matveev, K.M. Neyman, I.V. Yudanov, N. Rösch, Surf. Sci. 426 (1999) 123.
[14] Yu.F. Zhukovskii, E.A. Kotomin, P.W.M. Jacobs, A.M. Stoneham, Phys. Rev. Lett. 84 (2000) 1256;
Yu.F. Zhukovskii, E.A. Kotomin, P.W.M. Jacobs, A.M. Stoneham, J.H. Harding, J. Phys. Cond. Mat. 12 (2000) 55.
[15] N.C. Bacalis, A.B. Kunz, Phys. Rev. B 32 (1985) 4857.
[16] A.M. Ferrari, G. Pacchioni, J. Phys. Chem. 100 (1996) 9032.
[17] G. Pacchioni, N. Rösch, J. Chem. Phys. 104 (1996) 7329;
I.V. Yudanov, S. Vent, K.M. Neyman, G. Pacchioni, N. Rösch, Chem. Phys. Lett. 275 (1997) 245.
[18] N. Lopez, F. Illas, N. Rösch, G. Pacchioni, J. Chem. Phys. 110 (1999) 4873.
[19] U. Schönberger, O.K. Andersen, M. Methfessel, Acta Metall. Mater. 40 (1992) S1.
[20] C. Li, R. Wu, A.J. Freeman, C.L. Wu, Phys. Rev. B 48 (1993) 8317.
[21] J.R. Smith, T. Hong, D.J. Srolovitz, Phys. Rev. Lett. 72 (1994) 4121.
[22] R. Benedek, M. Minkoff, L.H. Yang, Phys. Rev. B 54 (1996) 7697.
[23] J. Goniakowski, Phys. Rev. B 57 (1998) 1935, 58 (1998) 1189.
[24] V. Musolino, A. Selloni, R. Car, Phys. Rev. Lett. 83 (1999) 3242.
[25] E. Heifets, Yu.F. Zhukovskii, E.A. Kotomin, M. Causá, Chem. Phys. Lett. 283 (1998) 395;
Yu.F. Zhukovskii, E.A. Kotomin, P.W.M. Jacobs, A.M. Stoneham, J.H. Harding, Surf. Sci. 441 (1999) 373;
Yu.F. Zhukovskii, E.A. Kotomin, D. Fuks, S. Dorfman, A. Gordon, Surf. Sci., in press.
[26] D.M. Duffy, J.H. Harding, A.M. Stoneham, Philos. Mag. A 67 (1993) 865;
Acta Metall. Mater. 43 (1995) 1559.
[27] J. Purton, S.C. Parker, D.W. Bullett, J. Phys. Cond. Mat. 9 (1997) 5709.
[28] J.A. Venables, Introduction to Surface and Thin Film Processes, Cambridge University Press, Cambridge, 2000.
[29] D. Frenkel, B. Smit, Understanding Molecular Simulations, Academic Press, San Diego, 1996;
I.K. Kamilov, A.K. Murtazaev, Kh.K. Aliev, Phys. Uspekhi 42 (1999) 689.
[30] A.M. Stoneham, in: P. Jena, C.B. Satterthwaite (Eds.), Electronic Structure and Properties of Hydrogen in Metals, Plenum Press, New York, 1983.
[31] D. Fuks, S. Dorfman, E.A. Kotomin, Yu.F. Zhukovskii, A.M. Stoneham, Phys. Rev. Lett. 85 (2000) 4333.
[32] M. Causá, R. Dovesi, C. Pisani, C. Roetti, Surf. Sci. 175 (1986) 551.
[33] E.A. Kotomin, V.N. Kuzovkov, Modern Aspects of Diffusion Controlled Reactions, Elsevier, Amsterdam, 1996.
[34] V.R. Saunders, R. Dovesi, C. Roetti, M. Causá, N.M. Harrison, R. Orlando, C.M. Zicovich-Wilson, CRYSTAL98 User Manual, University of Turin, 1999.
[35] M. Causá, A. Zupan, Int. J. Quant. Chem.: Quant. Chem. Symp. 28 (1994) 633;
M. Towler, A. Zupan, M. Causá, Comput. Phys. Commun. 98 (1996) 181.
[36] J.P. Perdew, Y. Wang, Phys. Rev. B 45 (1992) 13244.
[37] C. Lee, W. Yang, R.G. Parr, Phys. Rev. B 37 (1988) 785.
[38] J.P. Perdew, A. Zunger, Phys. Rev. B 23 (1981) 5048.
[39] S.H. Vosko, L. Wilk, M. Nusair, Can. J. Phys. 58 (1980) 1200.
[40] R.W. Grimes, C.R.A. Catlow, A.M. Stoneham, J. Phys. Cond. Mat. 1 (1989) 7367.
[41] K.A. Fichthorn, M. Scheffler, Phys. Rev. Lett. 84 (2000) 5371.
[42] E. Bauer, in: W. Schommers, P. von Blanckenhagen (Eds.), Structure and Dynamics of Surfaces II, Phenomena, Models and Methods, Springer-Verlag, Berlin, 1987, p. 115.
[43] G.H. Gilmer, in: R. Vanselow, R. Howe (Eds.), Chemistry and Physics of Solid Surfaces, Springer-Verlag, Berlin, 1984, p. 297.
[44] A.G. Khachaturyan, Theory of Structural Transformations in Solids, Wiley, New York, 1983.
[45] E.M. Lifshitz, Fiz. Zh. 7 (1942) 61, 7 (1942) 251;
L.D. Landau, E.M. Lifshitz, Statistical Physics, second ed., Pergamon Press, Oxford, 1978, English edition translated from Russian by J.B. Sykes and M.J. Kearsley.
[46] L. Kaufman, H. Bernstein, Computer Calculations of Phase Diagrams, Academic Press, New York, 1970.
[47] S.V. Semenovskaya, Phys. Status Solidi b 64 (1974) 291;
S.V. Semenovskaya, D.M. Umidov, Phys. Status Solidi b 64 (1974) 627;
S. Semenovskaya, A.G. Khachaturyan, Phys. Rev. B 51 (1995) 8409, 54 (1996) 7545.
[48] C.N.R. Rao, K.J. Rao, Phase Transitions in Solids, McGraw-Hill, New York, 1978.
[49] J.W. Cahn, J. Chem. Phys. 42 (1965) 93.
[50] P. Guenard, G. Renaud, B. Vilette, M.-H. Yang, C.P. Flynn, Scripta Metall. Mater. 31 (1994) 1221.
[51] D. Fuks, Z. Phys. B 104 (1997) 481.